Journal of Thermal Analysis and Calorimetry (2021) 146:2241–2251
https://doi.org/10.1007/s10973-020-10417-3

The CO_2 adsorption performance of aminosilane-modified mesoporous silicas

Muge Sari Yilmaz[1]

Received: 8 August 2019 / Accepted: 18 November 2020 / Published online: 4 January 2021

Abstract
Aminosilane-modified MCM-41 and SBA-15 mesoporous silicas were synthesized using sodium silicate extracted from gold mine tailings slurry in this study. Pure silica source was used in the synthesis of mesoporous silica in order to compare differences in textural properties and amine loading with differences in CO_2 adsorption performance. CO_2 adsorption analysis of the synthesized samples was carried out at 25, 75 and 100 °C. The results showed that the aminosilane-modified MCM-41 from slurry and aminosilane-modified SBA-15 from pure silica have the highest adsorption capacities of 1.55 and 1.37 mmol g^{-1}, respectively. As a result, it was found that the CO_2 adsorption capacities of the aminosilane-modified samples were increased by increasing the amine contents and the specific surface area. From three kinetic models (pseudo-first-order, pseudo-second-order model and Avrami's equation), Avrami model well represented the adsorption kinetic data for all adsorbents and revealed that multiple reaction pathway occurred in the CO_2 adsorption. In addition, aminosilane-modified samples presented good regenerability after four adsorption–desorption cycles.

Keywords Mesoporous silica · Tailings slurry · Alkali fusion · CO_2 adsorption · Kinetics

Introduction

CO_2 emissions increased day by day critically due to the excessive use of carbon-based fossil fuels [1]. In this case, serious concerns have been raised for the human activities and ecosystems. Therefore, the reducing the emissions of CO_2 into the atmosphere is an important issue. In recent years, many studies have been made to develop effective CO_2 capture technologies such as absorption in basic solutions, membrane purification, cryogenic distillations, and adsorption [2]. Among of them, adsorption has demonstrated great promise, due to its low energy requirements and easy operation [3]. Many materials have been developed as an adsorbent in CO_2 adsorption process such as membranes, metal–organic frameworks (MOF), physical adsorbents, chemical adsorbents, amine-grafted silicas, zeolites, ionic liquids, mesoporous materials, alkanolamines, and clathrate compounds [4]. Among the materials suitable for adsorption of CO_2, mesoporous silicas have received much attention on account of their desirable properties such as high surface area, large pore volume, uniform pore size, a long-range ordered pore structure, and facile functionalization [5, 6]. These materials have wide field of different areas from catalysts, adsorption, separation, and biomedical applications [7–12].

In the CO_2 adsorption process, it was observed that the modifying of the mesoporous silica with amine groups increased the adsorption capacity and selectivity with CO_2. Popa et al. conducted a study on effect of the amine type on thermal stability of modified mesoporous silica used for CO_2 adsorption. They found that adsorption capacity and the efficiency of amino groups depend on the type of amination reagents and the amount of organic compound used [13]. Barbosa et al. [14] reported that the used amine presented a pronounced influence for increasing the adsorption capacities of the mesoporous adsorbents used. Xu et al. [15] modified MCM-41 with branched polyethylenimine (PEI) including many amine sites. They found that CO_2 adsorption capacity of PEI-modified MCM-41 was much higher than pure MCM-41.

In this work, we prepared aminosilane-modified MCM-41 and SBA-15 from gold mine tailings slurry and pure silica

✉ Muge Sari Yilmaz
mugesari@yildiz.edu.tr

[1] Department of Chemical Engineering, Faculty of Chemical and Metallurgical Engineering, Yildiz Technical University, 34220 Istanbul, Turkey

sources to investigate of the CO_2 adsorption performance. The textural properties of the samples before and after modification were characterized, and the effects of amine content, textural properties, and adsorption temperature on the CO_2 adsorption performance of the samples were determined. Moreover, four adsorption–desorption cycles were carried out and the adsorption kinetics was also investigated.

Experimental

Materials and characterization

Gold mine tailings slurry was received from the Bergama Ovacık Gold Mine Treatment Plant, Turkey, and it was used as silica source. The slurry was dried at 105 °C for 2 h then ground and sieved under 90 µm. The chemical composition of the slurry was analyzed using X-ray fluorescence (XRF, PANalytical MiniPal4), and the Si, Al and Na concentrations of the extracted solution from the slurry were measured using inductively coupled plasma-optic emission spectrometry (ICP-OES, Perkin Elmer Optima 2100 DV). The chemical compositions of the slurry were 77.16% SiO_2, 13.01% Al_2O_3, 3.42% Fe_2O_3, 3.03% K_2O and 2.69% CaO.

X-ray diffraction (XRD) measurements were carried out at room temperature using a PANalytical Xpert Pro XRD instrument using Cu-Kα radiation ($\gamma = 1.540$ Å). Textural properties were determined by N_2 adsorption/desorption measurements using a Micromeritics ASAP2020 surface area and porosimetry analyzer. The specific surface area (S_{BET}) was calculated using the Brunauer–Emmett–Teller (BET) equation, and pore size distribution (PSD) was determined the Barrett–Joyner–Halenda (BJH) analyses using nitrogen desorption isotherms. The pure samples were degassed at 300 °C, while the aminosilane-modified samples were degassed at 120 °C in vacuum prior to the analysis. The thermal stability of silica samples was measured by a Perkin Elmer Pyris Diamond thermogravimetric analyzer with a heating rate of 10 °C min^{-1} in pure N_2 atmosphere. N contents of the samples were determined by elemental analysis using the LECO CHNS-932 instrument.

CO_2 adsorption/desorption measurements of the samples were performed by the same thermogravimetric analyzer for regenerability studies. High-purity CO_2 (> 99.99%) was used as an adsorptive gas in the adsorption/desorption measurement. The CO_2 adsorption experiments were performed at 25, 75, and 100 °C, while the CO_2 adsorption/desorption experiments were performed at 75 °C. Before CO_2 adsorption, approximately 10 mg of sample was loaded into an alumina crucible and heated to 105 °C under N_2 (100 mL min^{-1}) for 60 min to remove moisture. The temperature was then adjusted to the desired adsorption temperature, and the gas flow was changed from N_2 to CO_2 with a constant flow of 100 mL min^{-1} until there is no obvious change in sample mass. The change of the sample mass was measured for calculating of the adsorption capacity at the same time. After adsorption, the gas was switched to N_2 and the sample was cooled to a room temperature. The adsorption–desorption cycles were conducted at 75 °C and the CO_2 gas flow rate of 60 mL min^{-1}.

Synthesis of the samples

MCM-41 and SBA-15 from slurry derived silicate

In order to synthesize MCM-41 and SBA-15 from slurry-derived silicate, a fusion process was applied. In a typical preparation procedure, a given amount of slurry was mixed with NaOH and then, the mixture was calcined at 550 °C for 1 h. The obtained sample was dissolved in distilled water and then the mixture agitated for 24 h at room temperature. Finally,

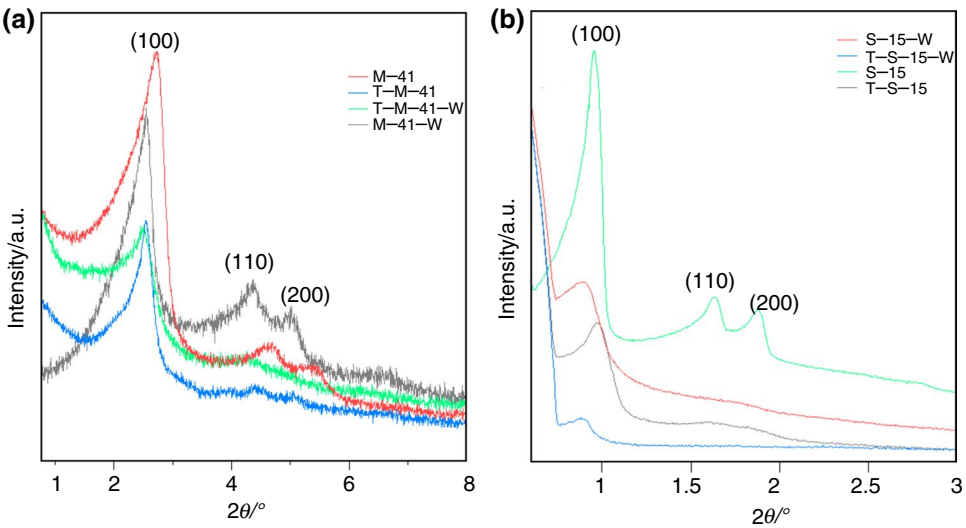

Fig. 1 XRD patterns of **a** MCM-41 and **b** SBA-15 adsorbents

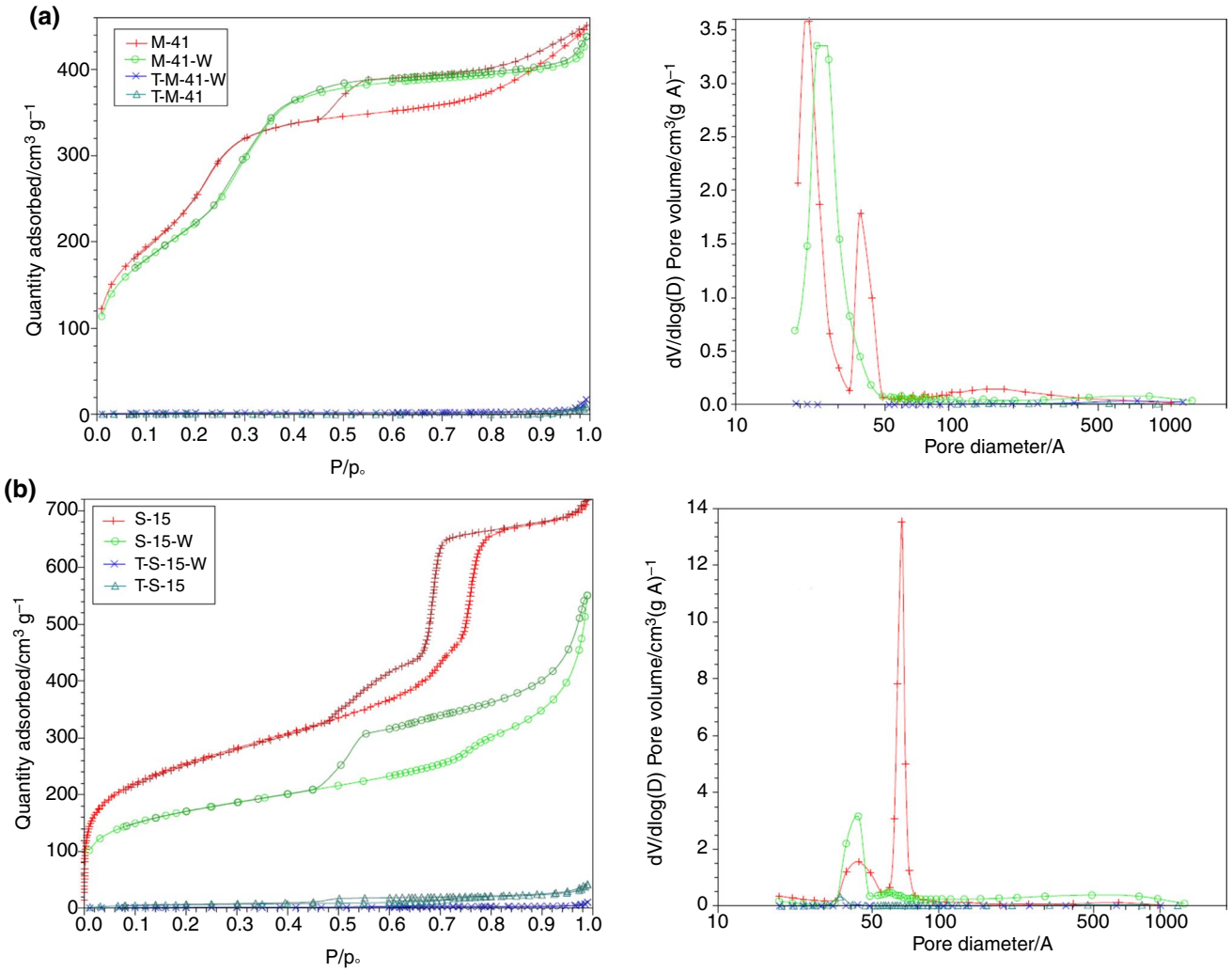

Fig. 2 N_2 adsorption/desorption isotherms and PSD curves of **a** MCM-41 and **b** SBA-15 adsorbents

Table 1 Textural properties and N contents of the synthesized samples

Name	S_{BET}/m^2 g^{-1}	d_{BJH}/nm[a]	V_p/cm^3 g^{-1}	N content/mass%
M-41-W	929.52	2.92	0.63	–
M-41	1046.55	2.96	0.66	–
T-M-41-W	7.35	26.87	0.01	7.97
T-M-41	2.50	31.76	0.01	7.46
S-15-W	582.13	6.83	0.61	–
S-15	887.88	5.66	1.06	–
T-S-15-W	5.21	12.42	0.01	6.74
T-S-15	22.91	7.37	0.04	8.00

[a]Pore diameter calculated by BJH theory

the solution was separated from the mixture by a filtration process [16, 17]. The Si, Al, and Na concentrations of the extracted silicate solution were 78,040 mg L^{-1}, 3600 mg L^{-1}, and 136,400 mg L^{-1}, respectively.

MCM-41 and SBA-15 derived from gold mine slurry were prepared according to our previous studies [18, 19]. The materials obtained accordingly were hereafter denoted as M-41-W and S-15-W, respectively. For comparison purpose, MCM-41 and SBA-15 from pure silica source tetraethyl orthosilicate (TEOS) were synthesized via the procedures previously described [18, 20]. The synthesized materials accordingly were hereafter denoted as M-41 and S-15, respectively.

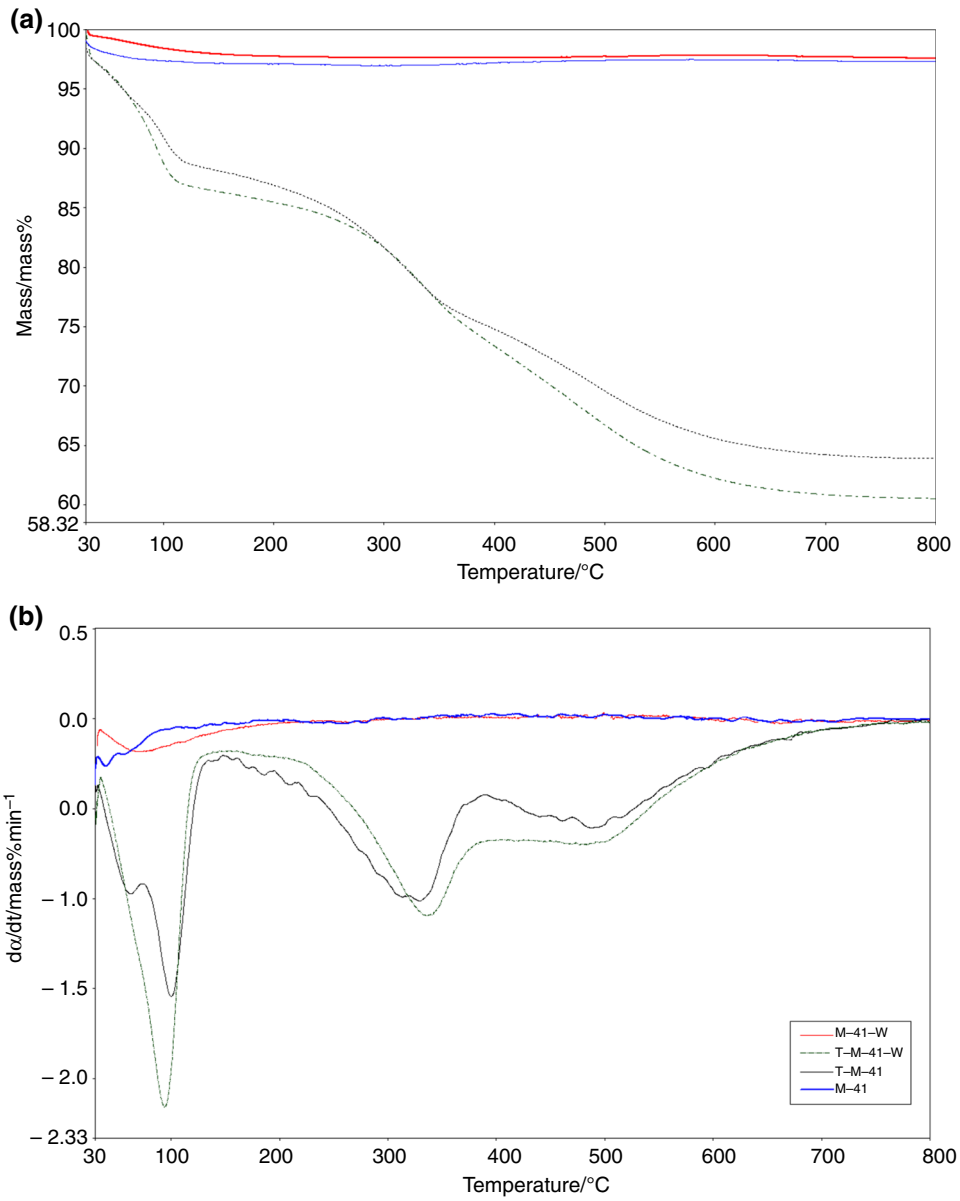

Fig. 3 TG and DTG curves of MCM-41

Aminosilane grafting

Aminosilane modifications of the synthesized samples were conducted by a chemical grafting method described before [8]. In a typical preparation, 0.5 g of dried adsorbent was dissolved and dispersed in dry toluene for 30 min with stirring. Then, 5 mL of N1-(3-trimethoxysilylpropyl) diethylenetriamine (TMPTA) was added to the mixture under stirring at room temperature and the resultant mixture refluxed for 6 h. The obtained sample was washed with dry toluene and dried at room temperature overnight. Amine-grafted MCM-41 samples synthesized from waste and pure silica were denoted as T-M-41-W and T-M-41, respectively. Amine-grafted SBA-15 samples synthesized from waste and pure silica were denoted as T-S-15-W and T-S-15, respectively.

Results and discussion

Characterization of samples

Figure 1 demonstrates the XRD results of the samples which were synthesized using sodium silicate supernatant from slurry and pure silica source. The patterns of MCM-41 exhibited in the three peaks were able to be indexed in (100), (110), and (200) reflections, which are characteristic of a well-ordered hexagonal mesostructure of MCM-41 (Fig. 1a). The peak intensities of the M-41 and M-41-W were decreased after the aminosilane modification. XRD patterns of the synthesized SBA-15 samples were given in Fig. 1b. The patterns of S-15 and T-S-15 show the characteristic diffraction peaks of highly ordered mesoporous

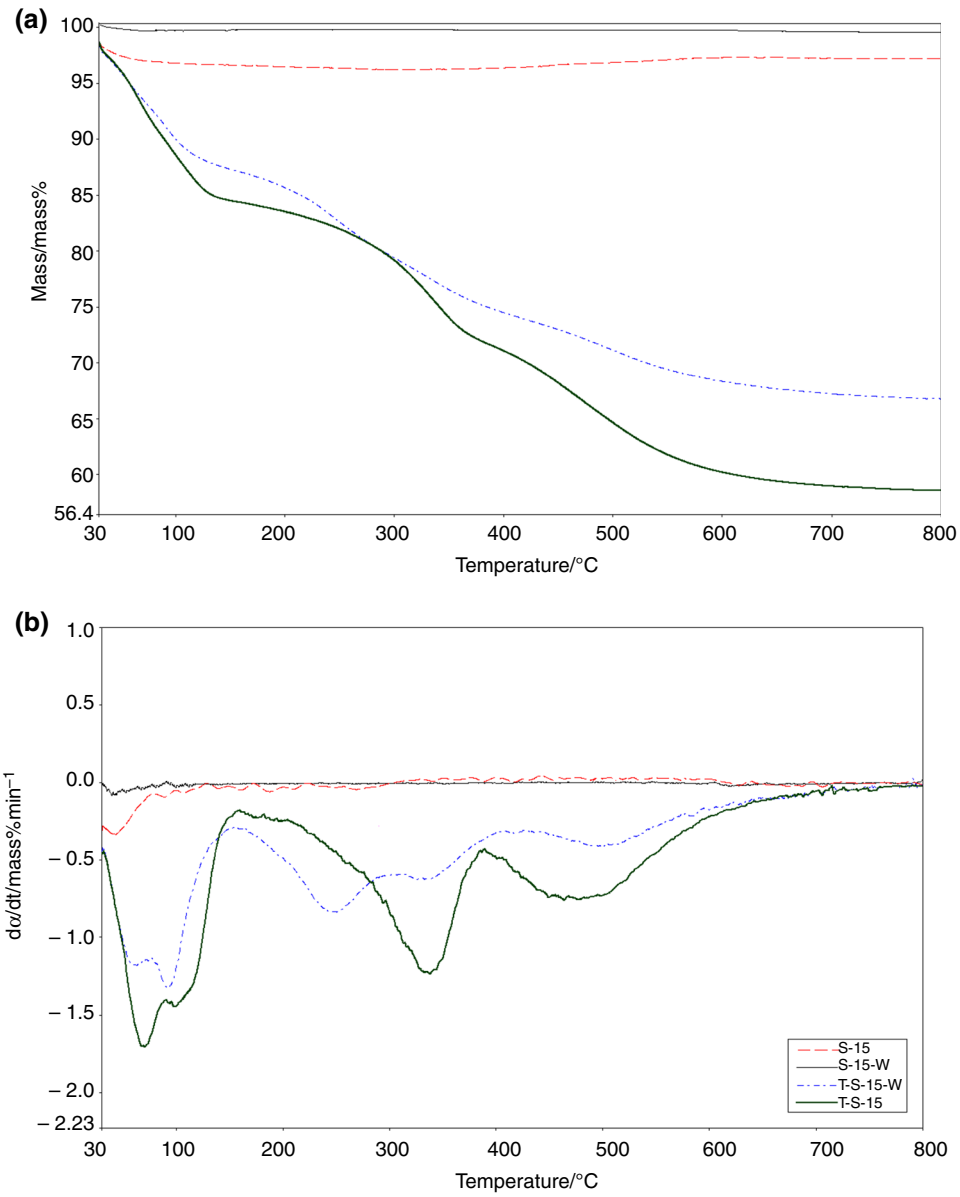

Fig. 4 TG and DTG curves of SBA-15

SBA-15, while XRD patterns of S-15-W and T-S-15-W reveal only the (100) reflection, indicating a less ordered pore structure. After aminosilane modification, the peak intensities of S-15 and S-15-W decreased significantly.

N_2 adsorption–desorption isotherms and pore size distribution (PSD) curves of MCM-41 and SBA-15 samples are shown in Fig. 2. All samples presented type-IV isotherms typical for MCM-41 and SBA-15 mesoporous silica samples. By modifying the silica surface with aminosilane, the values of specific surface area and pore volume of all samples decrease dramatically due to the pores of the samples being blocked/distorted by the amine groups (Table 1). The M-41 and S-15 were found to have the highest BET surface area (1046.55 and 887.88 m^2g^{-1}), while T-M-41 and T-S-15-W had the lowest BET surface area (2.50 and 5.21 m^2g^{-1}), as calculated from the adsorption isotherm. The PSD curve of M-41 shows two peaks centered at 2.21 and 4.35 nm, while M-41-W shows one peak centered at 2.47 nm. The PSD curve of S-15 exhibits one broad peak centered at 4.33 and one sharp narrow peak centered at 6.77 nm, while S-15-W shows one peak centered at 4.31 nm.

Thermogravimetric (TG) and differential thermogravimetric (DTG) curves of the synthesized samples are presented in Figs. 3 and 4. For M-41 and M-41-W, only one mass loss was found to occur between 30 °C and 115 °C, being attributed to the removal of physical adsorbed water. T-M-41 exhibited a three-stage mass loss, wherein one a mass loss of 8.93% occurred, due to the loss of physisorbed water (32–117 °C), in the other a mass loss of 13.61% occurred, due to decomposition of the organic

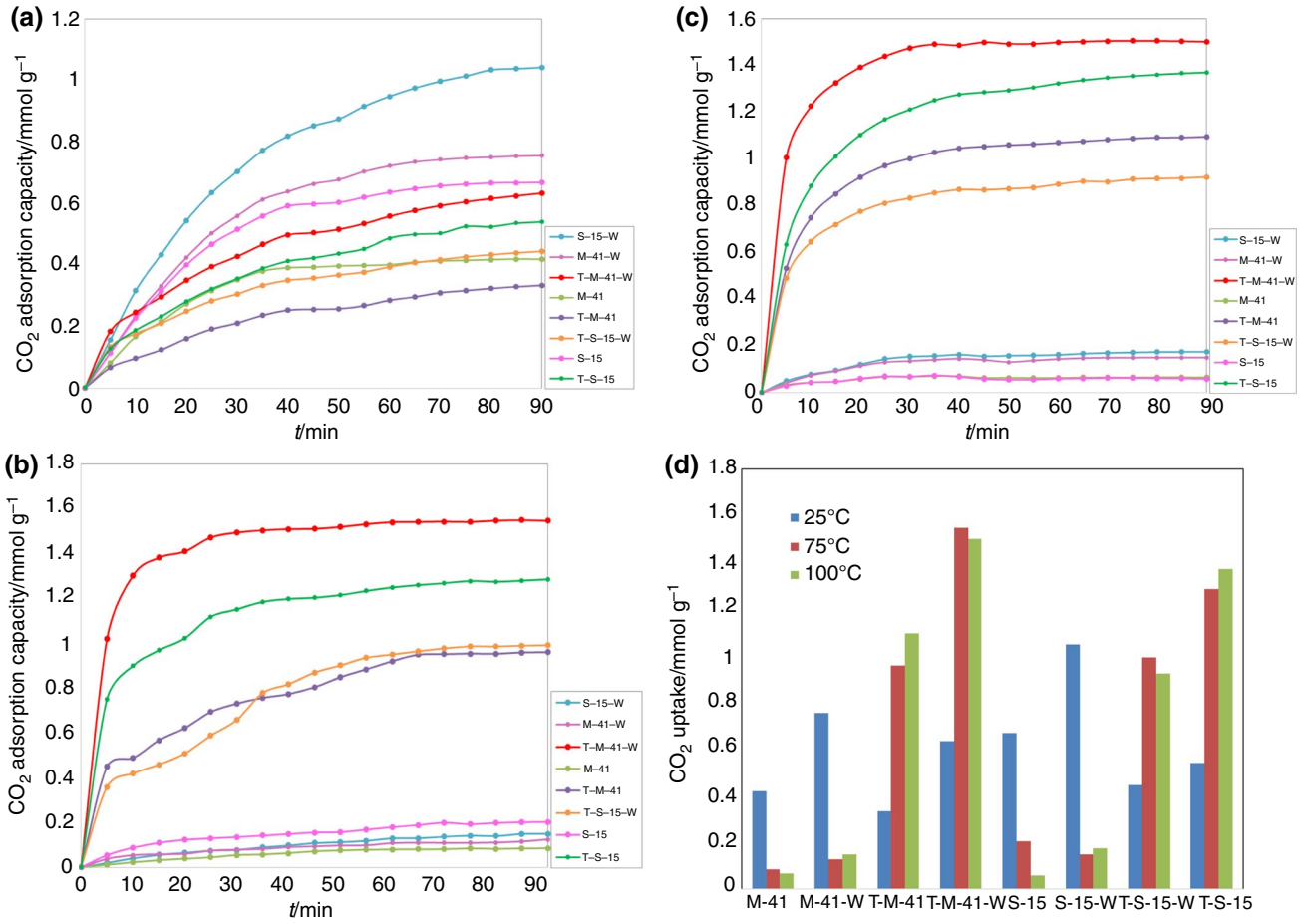

Fig. 5 CO_2 adsorption analysis of all samples at **a** 25, **b** 75, and **c** 100 °C. **d** Adsorption capacity comparison

Table 2 CO_2 adsorption capacity of triamine-modified sorbents from the literatures and this study

Support	*T*/°C	*P*/bar	CO_2 uptake/ mmol g^{-1}	Methods	References
KIT-6	30	1	1.89	Volumetric	[22]
SBA-15	30	1	1.54	Volumetric	[22]
MCM-41	30	1	1.36	Volumetric	[22]
MCM-41	30	1	1.01	Manometric gas dosing system	[23]
Precipitated silica	40	1	1.02	TG/DTA	[24]
Amorphous silica gel	20	1	1.05	TG/DTA	[25]
Hexagonal mesoporous silica	20	1	1.02	TG/DTA	[25]
Pore expanded -MCM-41	25	0.05	1.41	TG/DTA coupled with a mass spectrometer	[26]
HMS@Mg–Al LDH	75	1	1.28	TG/DTA	[9]
HMS	75	1	1.57	TG/DTA	[9]
T-M-41-W	75	1	1.55	TG/DTA	This work
T-S-15	100	1	1.37	TG/DTA	This work

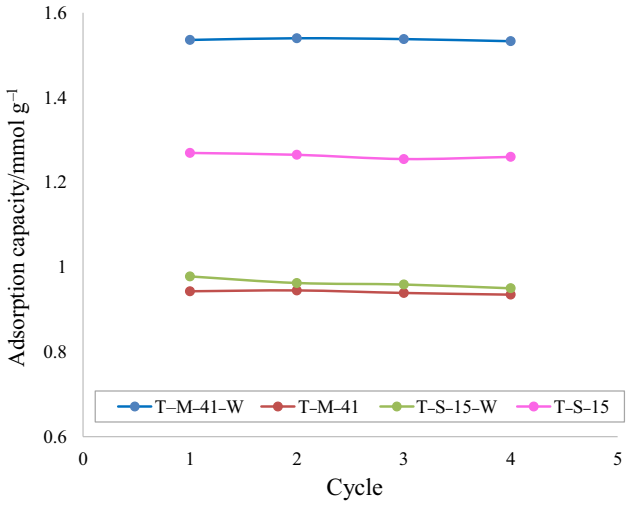

Fig. 6 Adsorption–desorption cycles for aminosilane-modified samples

species (117–386 °C), and in the other a mass loss of 11.46% occurred, due to decomposition of the remaining organic species (386–800 °C) [21]. T-M-41-W exhibited a three-stage mass loss, wherein one a mass loss of 10.44% occurred, due to the loss of physisorbed water (35–113 °C), in the other a mass loss of 13.04% occurred, due to decomposition of the organic species (113–388 °C), and in the other a mass loss of 13.61% occurred, due to decomposition of the remaining organic species (388–800 °C). For S-15 and S-15-W, only one mass loss was found to occur between 30 and 106 °C, being associated with physical adsorbed water on the surface of the materials. The thermal decomposition of T-S-15 took place in three separate stages. In the first stage, a mass loss of 11.92%, which was mainly the result of the removal of physical adsorbed water, occurred at temperatures below 120 °C; in the second stage, a mass loss of about 13.75% occurred at temperatures from 120 to 375 °C; and in the last stage, a mass loss of about 13.64% occurred, which can be attributed to the decomposition of the organic species at 800 °C [20]. For T-S-15-W, in the first stage, a mass loss of 9.61% occurred, due to removal of physical adsorbed water, at temperatures from 30 to 118 °C. In the second stage, a mass loss of 9.25% was observed between 118 and 303 °C, resulting from the decomposition of the organic species. Finally, in the last stage, at the temperature of 800 °C, there was a mass loss of 12.51%, caused by the decomposition of the remaining of the organic species. As expected, the total mass loss of aminosilane-modified samples was higher than the total mass loss of individual samples.

The total N contents of the aminosilane-modified samples were determined by elemental analysis, and results are also listed in Table 1. Although the same TMPTA amount was introduced to the all samples, the total N contents of the modified samples were different. This result may be due to different surface area that is able to accommodate more amine group.

CO_2 adsorption

Figure 5 demonstrates the CO_2 adsorption capacity of all the synthesized adsorbents at different temperatures. The samples reach the adsorption equilibrium in under ~ 70 min at 25 °C adsorption temperature, while the samples reach generally the adsorption equilibrium in under ~ 30 min at 100 °C. At 75 and 100 °C, the CO_2 uptake capacity of T-M-41-W is always the highest by comparing another adsorbents, while the uptake capacity of M-41 is the lowest by comparing another adsorbents. It was observed for all of the adsorbents, CO_2 adsorption capacities at 75 and 100 °C increased after the amine modification. On the contrary, the adsorption capacities at 25 °C for all adsorbents decreased after the amine modification despite of the reaction of CO_2 molecules with the amine groups (Fig. 5d). T-M-41-W and T-S-15 exhibited the highest CO_2 adsorption capacity at 75 °C and 100 °C. T-M-41-W presented the highest CO_2 uptake capacity of 1.55 mmol g^{-1} at 75 °C, almost 12.4 times greater than that of M-41-W and almost 1.6 times greater than that of T-M-41. T-S-15 presented the highest CO_2 uptake capacity of 1.37 mmol g^{-1} at 100 °C, almost 1.5 times greater than that of T-S-15-W and almost 23.2 times greater than that of S-15. M-41 and S-15 samples had the lowest CO_2 uptake performances at 100 °C. Moreover, T-M-41-W sample showed better performance for all adsorption temperatures in comparison with T-M-41 due to its higher amine content and higher the specific surface area. T-S-15 showed better performance for all temperatures in comparison with T-S-15-W due to its higher amine content and higher the specific surface area (Table 1). As a result, the adsorption capacity of the aminosilane-modified samples was strongly dependent on the amine contents and the specific surface area. In order to make a comparison, the CO_2 adsorption uptake of mesoporous materials modified with triamine, as reported in the literature, is summarized in Table 2. It can be observed that T-M-41-W and T-S-15 presented strong CO_2 adsorption performances.

The regenerability and cyclic stability of the sorbents are significant parameters for CO_2 capture materials in practical applications. Figure 6 shows the consecutive CO_2 adsorption–desorption cycles of the aminosilane-modified samples at 75 °C. From the figure, the adsorption capacities of the samples are similar in four adsorption–desorption cycles, demonstrating that the sorbents have a good regenerability and cyclic stability.

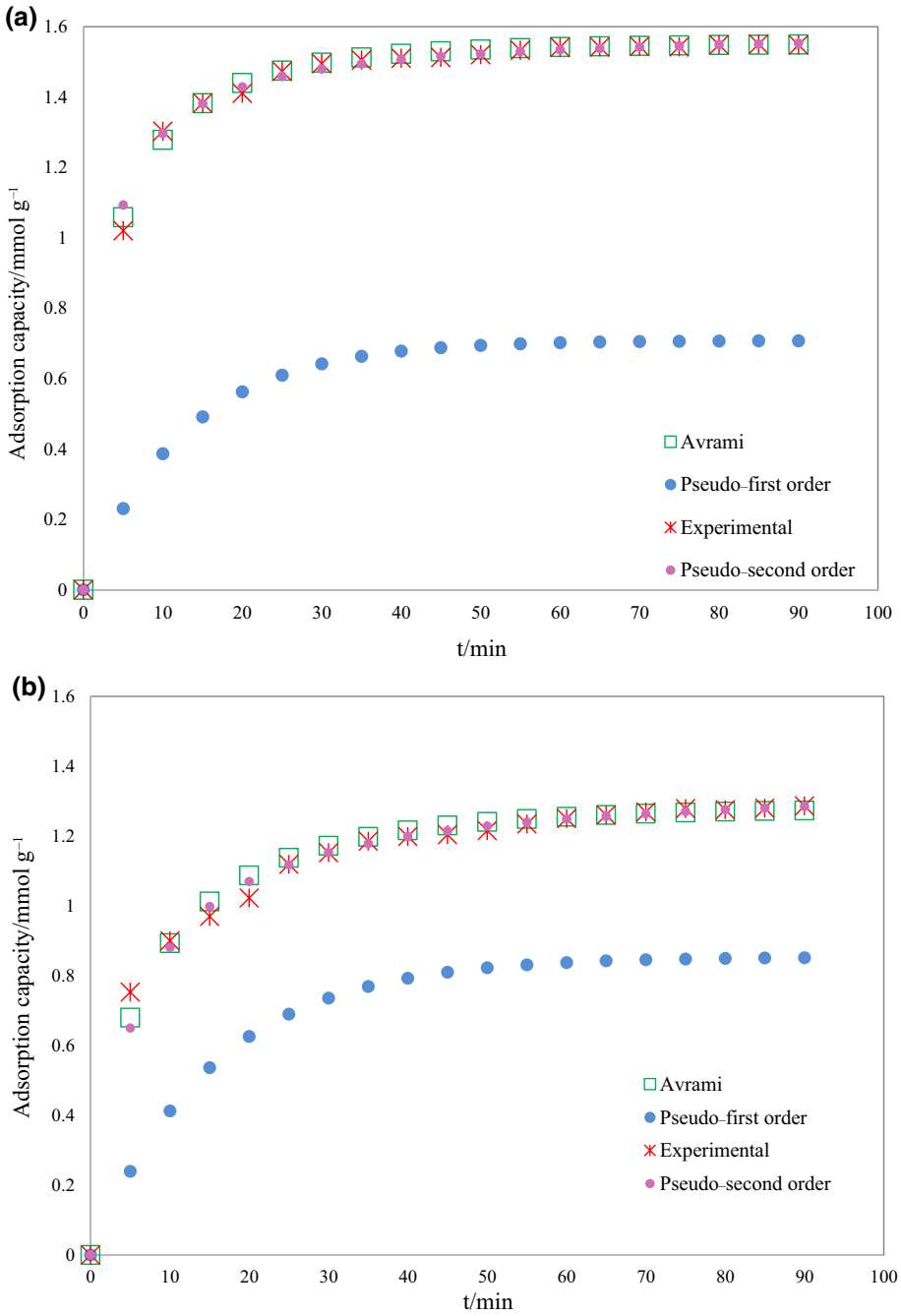

Fig. 7 The adsorption capacity of **a** T-M-41-W and **b** T-S-15 at 75 °C along with corresponding fit to the kinetic models

Kinetic study

Adsorption kinetics is an important issue for determining the mechanism of CO_2 adsorption on the sorbent. Accordingly, three adsorption kinetic models (pseudo-first-order, pseudo-second-order, and Avrami) were applied in this study. The pseudo-first-order kinetic model describes the kinetic process of sorption of the liquid/solid system. This model is represented by the following equation:

$$\frac{dq}{dt} = k_f \cdot (q_e - q_t) \quad (1)$$

where k_f is the pseudo-first order rate constant and q_e and q_t (mmol g^{-1}) are the adsorption capacities of equilibrium and a given time, respectively. For the boundary conditions of $q_t = 0$ at $t = 0$ and $q_t = q_e$ at $t = t_\infty$, Eq. 1 can be rearranged as:

$$q_t = q_e \cdot \left(1 - e^{(-k_f \cdot t)}\right) \quad (2)$$

Table 3 The kinetic models parameters for CO_2 adsorption over M-41 samples

Sample	*T*/°C	Pseudo-first-order				Pseudo-second-order				Avrami				
		q_e/mmol.g^{-1}	k_f/1.min^{-1}	Δq/%	R^2	q_e/mmol g^{-1}	k_S/g mmol^{-1} min^{-1}	R^2	Δq/%	q_e/mmol g^{-1}	k_A/1 min^{-1}	n	R^2	Δq/%
M-41-W	25	1.034	0.063	10.87	0.948	1.065	0.031	0.976	10.21	0.755	0.045	1.23	0.976	0.49
	75	0.126	0.076	8.46	0.847	0.145	0.309	0.979	11.01	0.107	0.069	0.72	0.967	3.29
	100	0.104	0.056	8.62	0.752	0.172	0.527	0.991	3.72	0.149	0.072	1.02	0.972	0.28
M-41	25	0.734	0.110	23.29	0.944	0.524	0.104	0.983	7.37	0.401	0.062	1.38	0.985	0.14
	75	0.093	0.049	6.05	0.928	0.136	0.152	0.972	17.07	0.085	0.041	1.22	0.971	2.28
	100	0.040	0.063	13.60	0.902	0.070	2.609	0.999	1.86	0.066	0.118	0.69	0.984	0.79
T-M-41-W	25	0.954	0.487	16.88	0.953	0.784	0.055	0.993	7.59	0.639	0.048	0.79	0.984	2.45
	75	0.708	0.079	15.85	0.939	1.592	0.275	1.000	0.78	1.551	0.251	0.60	0.984	0.20
	100	1.231	0.137	7.154	0.979	1.549	0.316	1.000	0.90	1.516	0.230	0.68	0.993	0.82
T-M-41	25	0.335	0.043	2.19	0.964	0.467	0.059	0.989	11.87	0.332	0.040	0.99	0.980	1.98
	75	0.822	0.049	3.90	0.931	1.115	0.064	0.992	4.10	1.021	0.059	0.73	0.977	2.65
	100	0.814	0.080	7.03	0.994	1.164	0.167	1.000	1.91	1.083	0.120	0.80	0.998	0.17

Table 4 The kinetic models parameters for CO_2 adsorption over S-15 samples

Sample	*T*/°C	Pseudo-first-order				Pseudo-second-order				Avrami				
		q_e/mmol g^{-1}	k_f/1 min^{-1}	Δq/%	R^2	q_e/mmol g^{-1}	k_S/g mmol^{-1} min^{-1}	R^2	Δq/%	q_e/mmol g^{-1}	k_A/1 min^{-1}	n	R^2	Δq/%
S-15-W	25	1.237	0.052	6.65	0.957	1.508	0.018	0.993	12.04	1.033	0.042	1.14	0.993	1.01
	75	0.176	0.041	6.34	0.930	0.242	0.075	0.985	16.53	0.154	0.033	1.05	0.987	2.58
	100	0.135	0.054	5.72	0.901	0.202	0.371	0.993	4.47	0.174	0.061	0.91	0.982	0.79
S-15	25	0.854	0.062	7.72	0.958	0.892	0.044	0.983	8.14	0.671	0.047	1.17	0.993	0.34
	75	0.161	0.035	5.47	0.927	0.249	0.181	0.982	5.75	0.232	0.043	0.62	0.984	5.28
	100	0.020	0.040	23.86	0.315	0.062	11.494	0.983	0.37	0.062	0.120	0.69	0.993	0.73
T- S-15-W	25	0.947	0.921	42.30	0.991	0.547	0.082	0.993	9.17	0.411	0.053	1.00	0.988	1.40
	75	1.336	0.060	9.44	0.942	1.271	0.035	0.978	6.78	0.999	0.040	1.35	0.977	0.37
	100	0.528	0.057	11.28	0.958	0.973	0.200	1.000	1.52	0.927	0.135	0.63	0.992	0.39
T- S-15	25	0.569	0.043	2.26	0.967	0.711	0.049	0.994	8.35	0.555	0.039	0.99	0.982	1.73
	75	0.854	0.066	8.95	0.967	1.363	0.134	1.000	1.93	1.281	0.131	0.66	0.989	0.55
	100	0.989	0.064	7.40	0.977	1.473	0.103	1.000	2.18	1.365	0.105	0.74	0.991	0.35

The pseudo-second-order kinetic model is based on the rate of the adsorption being proportional to the square of the number of unoccupied adsorption sites on the adsorbent surface. It can be expressed by Eq. 3.

$$\frac{dq}{dt} = k_s \cdot \left(q_e - q_t\right)^2 \tag{3}$$

where k_s is the pseudo-second-order rate constant. For the boundary conditions of $q_t = 0$ at $t = 0$ and $q_t = q_e$ at $t = t_\infty$, Eq. 3 can be rearranged as:

$$q_t = \frac{q_e^2 k_s t}{1 + q_e k_s t} \tag{4}$$

The Avrami model was applied to describe the CO_2 gas uptake rate on the functionalized adsorbents [10]. It can be calculated as follows:

$$\frac{dq}{dt} = k_A^n \cdot t^{n-1} \cdot \left(q_e - q_t\right) \tag{5}$$

where k_A is the Avrami kinetic constant and n is the Avrami exponent. For the boundary conditions of $q_t = 0$ at $t = 0$ and $q_t = q_e$ at $t = t_\infty$, Eq. 5 can be rearranged as:

$$q_t = q_e \cdot \left(1 - e^{-(k_A \cdot t)^n}\right) \tag{6}$$

An error function ($\Delta q/\%$) was determined in order to verify the accuracy of the model. It can be expressed by the following equations:

$$\Delta q(\%) = \sqrt{\frac{\Sigma\left[\frac{q_{e(exp)} - q_{e(pred)}}{q_{e(exp)}}\right]^2}{N - 1}} \times 100\% \tag{7}$$

where N is the number of experimental data points on the kinetic curve and $q_{e(exp)}$ and $q_{e(pred)}$ are the experimental and predicted adsorption capacity values, respectively.

The fitting results of experimental data for T-M-41-W and T-S-15 exhibited highest adsorption capacities are demonstrated in Fig. 7. The parameters of the adsorption kinetic models are listed in Tables 3 and 4. According to the correlation coefficient (R^2) values for all samples, the pseudo-second-order kinetic model provides the best fitting of the three models followed by Avrami model. However, Avrami kinetic model presented a lower value of $\Delta q/\%$ than the errors calculated from the pseudo-first-order and pseudo-second-order models. Also, by looking at the fitted data (Fig. 7), it can be seen that the fitted data from Avrami kinetic model for T-M-41-W and T-S-15 were very close to the experimental data. The values of the Avrami exponents for all the samples were within the range of 0.6–1.4, revealing that multiple reaction pathway occurred in the CO_2 adsorption.

Conclusions

Mesoporous silicas MCM-41 and SBA-15 were synthesized from gold mine tailings slurry and TEOS as silica precursors. The synthesized samples were further modified with aminosilane to prepare the sorbents for CO_2 adsorption. T-M-41-W has the highest adsorption capacity of 1.55 mmol g^{-1} at 75 °C, while T-S-15 demonstrates the highest adsorption capacity of 1.37 mmol g^{-1} at 100 °C. As a result of analysis, it was seen that the amine content and the specific surface area were the factor influencing the CO_2 adsorption capacities of the aminosilane-modified samples. The amine-modified samples revealed well regenerability after four adsorption–desorption cycles. The Avrami model provided the best fit to the experimental data for the kinetics of CO_2 adsorption on all of the samples and suggested that multiple reaction pathway occurred in the CO_2 adsorption.

References

1. Yaumi A, Bakar MA, Hameed B. Recent advances in functionalized composite solid materials for carbon dioxide capture. Energy. 2017;124:461–80.
2. Leung DY, Caramanna G, Maroto-Valer MM. An overview of current status of carbon dioxide capture and storage technologies. Renew Sustain Energy Rev. 2014;39:426–43.
3. Harrison DP. The role of solids in CO2 capture: a mini review. In: Greenhouse gas control technologies, vol 7. Elsevier; 2005. p. 1101-6.
4. D'Alessandro DM, Smit B, Long JR. Carbon dioxide capture: prospects for new materials. Angew Chem Int Ed. 2010;49(35):6058–82.
5. Jafari S, Derakhshankhah H, Alaei L, Fattahi A, Varnamkhasti BS, Saboury AA. Mesoporous silica nanoparticles for therapeutic/diagnostic applications. Biomed Pharmacother. 2019;109:1100–11.
6. Isa EDM, Mahmud IS, Ahmad H, Rahman MBA. Dependence of mesoporous silica properties on its template. Ceram Int. 2019;45(9):12149–53.
7. Yilmaz SM, Özdemir ÖD, Pişkin S. Synthesis and characterization of MCM-41 with different methods and adsorption of Sr 2+ on MCM-41. Res Chem Intermed. 2015;41(1):199–211.
8. Yilmaz SM, Palantoken A, Piskin S. Release of flurbiprofen using of SBA-15 mesoporous silica: influence of silica sources and functionalization. J Non-Cryst Solids. 2016;437:80–6.
9. Yilmaz SM. Synthesis of novel amine modified hollow mesoporous silica@ Mg–Al layered double hydroxide composite and its application in CO_2 adsorption. Microporous Mesoporous Mater. 2017;245:109–17.
10. Yilmaz SM, Karakas SB. Low-cost synthesis of organic-inorganic hybrid MSU-3 from gold mine waste for CO_2 adsorption. Water Air Soil Pollut. 2018;229(10):326.
11. Jafari S, Maleki-Dizaji N, Barar J, Barzegar-Jalali M, Rameshrad M, Adibkia K. Physicochemical characterization and in vivo evaluation of triamcinolone acetonide-loaded hydroxyapatite nanocomposites for treatment of rheumatoid arthritis. Colloids Surf B. 2016;140:223–32.

12. Samanta PK, Ray S, Das T, Gage SH, Nandi M, Richards RM, et al. Palladium oxide nanoparticles intercalated mesoporous silica for solvent free acceptorless dehydrogenation reactions of alcohols. Microporous Mesoporous Mater. 2019;284:186–97.
13. Popa A, Sasca V, Verdes O, Suba M, Barvinschi P. Effect of the amine type on thermal stability of modified mesoporous silica used for CO_2 adsorption. J Therm Anal Calorim. 2018;134(1):269–79.
14. Barbosa MN, Araujo AS, Galvão LP, Silva EF, Santos AG, Luz GE, et al. Carbon dioxide adsorption over DIPA functionalized MCM-41 and SBA-15 molecular sieves. J Therm Anal Calorim. 2011;106(3):779–82.
15. Xu X, Song C, Andresen JM, Miller BG, Scaroni AW. Preparation and characterization of novel CO2 "molecular basket" adsorbents based on polymer-modified mesoporous molecular sieve MCM-41. Microporous Mesoporous Mater. 2003;62(1–2):29–45.
16. Shigemoto N, Hayashi H, Miyaura K. Selective formation of Na-X zeolite from coal fly ash by fusion with sodium hydroxide prior to hydrothermal reaction. J Mater Sci. 1993;28(17):4781–6.
17. Yilmaz SM, Mermer NK. Conversion of fly ashes from different regions to mesoporous silica: effect of the mineralogical composition. J Sol-Gel Sci Technol. 2016;78(2):239–47.
18. Degitz IA, Yilmaz SM, Piskin S. Recycle of gold mine tailings slurry into MCM-41 mesoporous silica with high specific surface area. Chem Ind Chem Eng Q. 2017;23(4):581–8.
19. Yilmaz SM, Piskin S. Evaluation of novel synthesis of ordered SBA-15 mesoporous silica from gold mine tailings slurry by experimental design. J Taiwan Inst Chem Eng. 2015;46:176–82.
20. Yilmaz SM, Piskin S. The removal of template from SBA-15 samples synthesized from different silica sources. J Therm Anal Calorim. 2015;121(3):1255–62.
21. Yilmaz SM, Degitz IA, Piskin S. Thermal analysis applied for the removal of surfactant from mesoporous molecular sieves MCM-41 synthesized from gold mine tailings slurry. J Therm Anal Calorim. 2017;130(2):727–34.
22. Kishor R, Ghoshal AK. N 1-(3-Trimethoxysilylpropyl) diethylenetriamine grafted KIT-6 for CO 2/N 2 selective separation. RSC Adv. 2016;6(2):898–909.
23. dosSantos TC, Bourrelly S, Llewellyn PL, Carneiro JWdM, Ronconi CM. Adsorption of CO2 on amine-functionalised MCM-41: experimental and theoretical studies. Phys Chem Chem Phys. 2015;17(16):11095–102.
24. Li K-M, Jiang J-G, Tian S-C, Chen X-J, Yan F. Influence of silica types on synthesis and performance of amine-silica hybrid materials used for CO2 capture. J Phys Chem C. 2014;118(5):2454–62.
25. Knowles GP, Delaney SW, Chaffee AL. Diethylenetriamine [propyl (silyl)]-functionalized (DT) mesoporous silicas as CO2 adsorbents. Ind Eng Chem Res. 2006;45(8):2626–33.
26. Harlick PJ, Sayari A. Applications of pore-expanded mesoporous silicas: 3—Triamine silane grafting for enhanced CO2 adsorption. Ind Eng Chem Res. 2006;45(9):3248–55.